Seasonal responses of $\delta^{13}C$ and $\delta^{18}O$ of atmospheric CO_2 over sub-urban region of India

Mahesh Pathakoti[1*], A.L. Kanchana[1], Aarathi Ramesh Muppalla[2], D.V. Mahalakshmi[1], Vijay Kumar Sagar[1,3] , Sreenivas G[4] and P.Raja[5]

[1]Analytics and Modelling Division (AMD), Earth and Climate Systems Study Division (ECSSD), Land and Atmospheric Physics Division (LAPD), Atmospheric Chemistry Division (ACD), Earth and Climate Sciences Area (ECSA), National Remote Sensing Centre (NRSC), Indian Space Research Organization (ISRO), Hyderabad-500037, India.

[2]Bhuvan Project Management and Software Evaluation Division, Bhuvan Geoportal and Data Dissemination Area, National Remote Sensing Centre (NRSC), Indian Space Research Organization (ISRO), Hyderabad-500037, India.

[3]Centre for Earth, Ocean and Atmospheric Sciences, University of Hyderabad, 500084, India.

[4]Department of Physics, Jawaharlal Nehru Technological University, Hyderabad, 500085, India

[5]ICAR-Indian Institute of Soil and Water Conservation, Research Centre,Ooty, The Nilgiris, Tamil Nadu, - 643004, India.

*Corresponding author: Mahesh Pathakoti (mahi952@gmail.com)

Key Points:

- Study focused on diurnal variability of seasonal atmospheric CO_2 and its stable isotopes ($\delta^{13}C$ and $\delta^{18}O$).
- Determination of $\delta^{13}C$ signature of atmospheric CO_2 using improved Miller and Tans model.
- Effect of the Indian Summer monsoon circulation on atmospheric CO_2 variation was studied.

Abstract

The seasonal diurnal variability of atmospheric CO_2 and driving factors are studied using its continuous isotopic fractionation ($\delta^{13}C$ and $\delta^{18}O$) over Shadnagar, a sub-urban location of India with high precision *in-situ* data from November 2018 to October 2019. The annual averaged atmospheric CO_2 concentrations and ^{13}C-CO_2 and ^{18}O-CO_2 are 415.03±9.77 ppm, -11.18±1.73 ‰ and 9.1±13.35 ‰. Seasonal amplitudes of atmospheric CO_2 was observed in summer monsoon (17.30 ± 9.29 ppm) and the minimum was noticed in winter (7.19 ± 0.11 ppm) indicating strong seasonality at the study site. To characterize the atmospheric CO_2 sources/sinks, an improved model of Miller and Tans was implemented by plotting ΔCO_2 against $\Delta(CO_2 \times \delta^{13}C)$ respectively during day and night. An averaged seasonal $\delta^{13}C$ source/sink signature (δ_s) is -32.84 ‰ in the

day time and -26.09‰ in night time representing the source of atmospheric CO_2 is related to combustion and dominance of C_3 ecosystem respiration respectively. The seasonal relationship between $\delta^{18}O$ and $\delta^{13}C$ is strongly correlated during pre-monsoon ('r' = 0.93 to 0.95) than post-monsoon ('r' = 0.07 to 0.13), which might be due to high vapour pressure deficit. A Lagrangian back-trajectory model confirms the influence of the Indian Summer Monsoon on the variability of atmospheric CO_2 concentration during the summer monsoon season.

Keywords: atmospheric CO_2, isotopic fractionation, Miller and Tans, Indian summer monsoon.

1. Introduction

The Intergovernmental Panel for Climate Change (IPCC) reported that carbon dioxide (CO_2) sources from anthropogenic gases in the atmosphere cause more radiative forcing next to water vapor (Smith et al., 1999). CO_2 concentrations are consistently increasing and touched 400 ppm at Mauna Loa, a global reference site during May 2013 (Monastersky, 2013). Globally, CO_2 concentrations are increasing, which could be due to land use land cover changes (LULCC) and progress in industrial activities (Ballantyne et al., 2012) especially fossil fuel combustion, cement manufacturing. Due to fossil fuels burnings and LULC emissions, an increase of 40 and 150 % in CO_2 and CH_4 concentration respectively is observed since the pre-industrial period (Huang et al., 2016). Emissions of CO_2 by different processes are controlled by varied environmental conditions, in which about half of the CO_2 levels are released into the atmosphere as source and remaining are absorbed by the processes of the terrestrial biosphere and ocean uptake (Andres et al., 1996) as sink. Hence monitoring and maintaining long-term records of atmospheric CO_2 measurements are very important to understand the carbon cycle and to assess the CO_2 mixing ratios in the atmosphere by controlling factors namely photosynthesis, respiration, biomass, fossil fuel burning and air-sea exchange processes (Machida et al., 2003).

Globally, systematic high precision atmospheric CO_2 observations are accelerated to understand the global carbon cycle. Over the Indian subcontinent, spatio-temporal variability in atmospheric CO_2 concentrations are characterized by the terrestrial biosphere and seasonal weather patterns which brings long-range air-masses (Valsala et al., 2013; Tiwari et al., 2014). To understand the seasonal, inter and intra annual variations of atmospheric CO_2 over the Indian subcontinent, high precision CO_2 measurements are being generated across the country from different research institutes (Bhattacharya et al., 2009; Sharma et al., 2014; Mahesh et al., 2016; Nalini et al., 2019). A literature survey on atmospheric CO_2 variability over the Indian region is mainly focused on local sources and transport (Sreenivas et al., 2016). However, a need was felt to understand the reasons and causes for uncertainty in surface fluxes. Hence an advanced studies of stable isotopic measurements of carbon and oxygen are gaining momentum to understand CO_2 levels, source and sinks of CO_2, both on regional and global levels.

Stable carbon and oxygen isotopes of atmospheric CO_2 can be used as tracers in the carbon cycle, which are affected by the anthropogenic and biogenic CO_2 components. The ^{13}C-CO_2 and ^{18}O-CO_2 are stable isotopes of CO_2 molecules are widely used for source apportionments in the atmosphere, hydrosphere and geosphere as well as interaction between them (Guillon et al., 2015). The ^{13}C-CO_2 concentration in the atmosphere has been decreasing since pre-industrial times, which indicates the more addition of CO_2 to the atmosphere by fossil fuel burning (Yakri, 2011). Many research activities have been carried out on atmospheric CO_2 and its stable isotopes ($\delta^{13}C$, $\delta^{18}O$) by various groups (Bhattacharya et al., 2009; Pataki et al., 2003; Clark-Thorne and

yapp, 2003; Francey and Tans, 1987; Murayama et al., 2010; Newman et al, 2003; Wada et al., 2011; Pataki et al., 2006; Zhou et al., 2005; Zhou et al., 2006; Sturm et al., 2006; Djuricin et al., 2010; Guha and Ghosh, 2010; Gorka and Lewicka- Szczebak, 2013; Liu et al., 2014a; Pang et al., 2016). Liu et al. (2014a) studied the atmospheric CO_2, $\delta^{13}C$ composition and their relationship to understand the sources and sinks at two stations viz., Waliguan and Shangdianzi in China using observational data for the period from 2007 to 2010. The result of this study indicates that CO_2 and $\delta^{13}C$ composition possesses long-term trends and seasonal cycles that correlate with each other. An improved model by Miller and Tans (2003) is widely used to determine the source or sink that causes CO_2 variability. Pang et al. (2016) used Keeling plot intercept method for isotopic composition of CO_2 and found increased value in vegetative season and depleted value in heating season. On Indian sub-continent a few studies are carried out on atmospheric CO_2 and its stable isotopes which are limited to discrete sample analysis (Bhattacharya et al., 2009; Guha and Ghosh, 2015). Measurements of the ^{18}O-CO_2 also play an important role in the carbon cycle to distinguish the photosynthesis and respiration process of CO_2 fluxes (Farquhar et al., 1993; Kato et al., 2004).

The objective of the present study is to understand seasonal diurnal variability of atmospheric CO_2 and its stable isotopic composition at the sub-urban region of Telangana. Since the study site is surrounded by multiple sources for CO_2 (e.g., biospheric respiration and fossil fuel emissions), thus an improved model by Miller and Tans (2003) was used to characterize the CO_2 sources/sinks. Here, we report continuous high precision CO_2 isotopic measurements, first of their kind from sub-urban region of Telangana. This work has been carried out as part of the Atmospheric CO_2 Retrieval and Monitoring (ACRM) of National Carbon Project (NCP) funded by Climate and Atmospheric Processes of ISRO-Geosphere Biosphere Programme (CAP-IGBP).

2. Materials and Methods

Observations of CO_2 and its isotopic composition are measured during November 2018 to October 2019 by laser based Isotope Ratio Infrared Spectrometer (IRIS) analyser at 8 m height from the surface of Atmospheric Science Laboratory (ASL), NRSC, Shadnagar (Latitude: 17.09 °N; Longitude: 78.21 °E and Elevation: 648 m above mean sea level) a sub-urban region of Telangana. Surface meteorological data at the study site are collected from an automatic weather station. An hourly Boundary Layer Height (BLH) were obtained from European Centre for Medium- Range Weather Forecasts (ECMWF-ERA, https://cds.climate.copernicus.eu/cdsapp#!/dataset/reanalysis-era5-single-levels?tab=form). In addition to the above datasets, fire counts with confidence > 70% are obtained from Moderate Resolution Imaging Spectroradiometer (MODIS, https://firms.modaps.eosdis.nasa.gov/download/). Normalized Difference vegetation Index (NDVI) is obtained from an open data archival of Bhuvan site (https://bhuvan-app3.nrsc.gov.in/data/download/index.php), which is derived from Oceansat-2 Ocean color monitor sensor. Figure 1a shows that the study area is overlaid with NDVI over Telangana state as well as time series of air temperature, relative humidity and wind speed recorded at the study site.

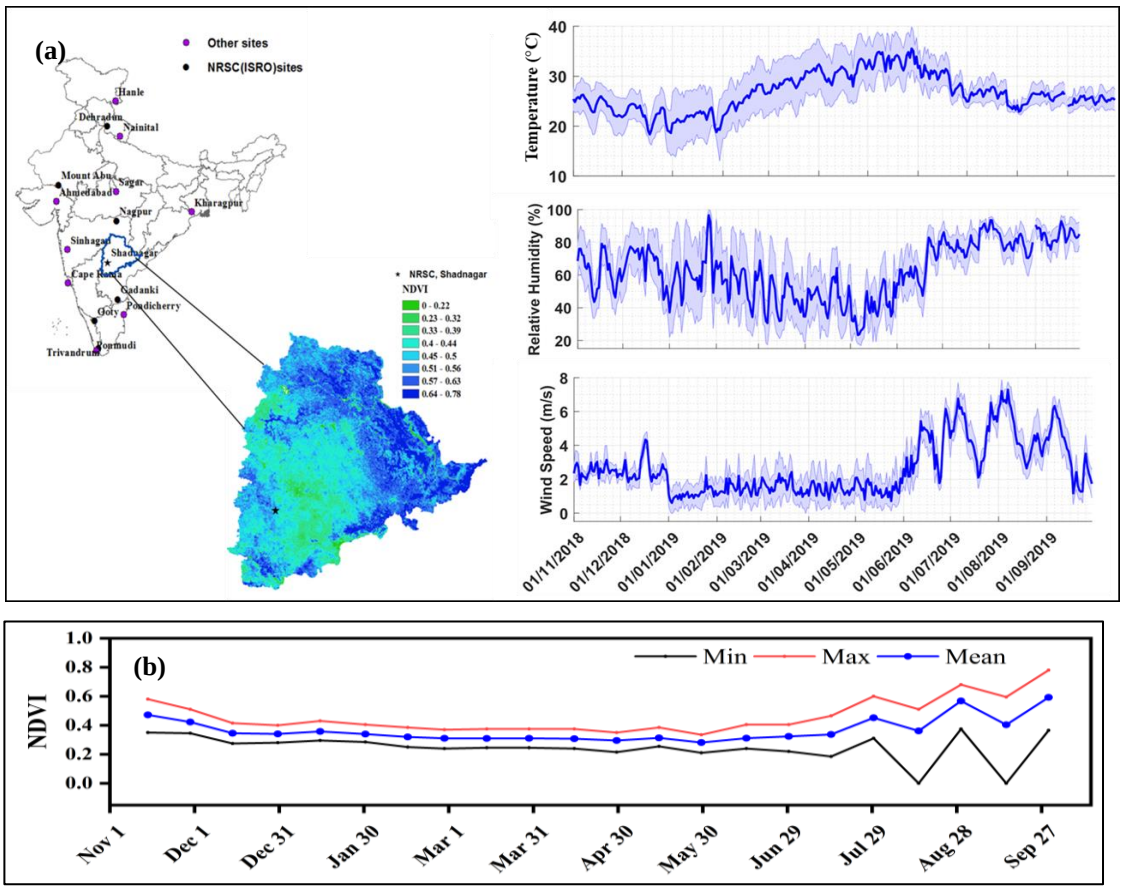

Figure 1. (a) Study location with prevailing weather conditions and (b) NDVI

Figure 1a also shows *in-situ* atmospheric CO_2 networks across the country established by different research institutes of India. A few of the station's information is obtained from Nalini et al. (2019). Black solid circles are the atmospheric CO_2 measurement stations installed under ACRM of NCP project by NRSC, ISRO. At the present study site (solid black star) long-term CO_2, CH_4 and H_2O measurements are complemented by CO_2 and N_2O isotopic observations. During the study period, air temperature is observed to be high in pre-monsoon (March-May) with maximum air temperature of 43°C and low in winter (January-February) with mininum temperature of 9°C. Relative humidity is observed to be high in monsoon (June-September) with maximum value reaching 100 % and low in pre-monsoon with minimum of 12.18 %. However, wind speed is observed to be ranging from 0.005 m s^{-1} to 6.0 m s^{-1} during the study period. Figure 1b shows minimum, maximum and mean NDVI at 15-day interval at the study site. Thus, seasonal NDVI are computed during the study period for post-monsoon (0.39), winter (0.33), pre-monsoon (0.30) and monsoon (0.41). The study site is about 60 km away from the urban region of Hyderabad (fifth largest city in India) and is associated with 75% air pollution from traffic sector alone (significant anthropogenic impacts) due to increase in population and related factors (Malakshmi et al., 2014). Thus the present study site doesn't fall under single source contributor of atmospheric CO_2.

2.1. Continuous stable isotopic measurements

In this study, we used commercial laser based IRIS CO_2 Carbon Isotope analyzer Enhanced Performance (CO_2-CCIA-EP), procured from Los Gatos Research, U.S.A in November 2018. Details of the instrument functioning are given in Baer et al. (2002). The CO_2-CCIA-EP is capable of simultaneous measurements of dry CO_2, ^{13}C, ^{18}O and H_2O are measured using the absorption line at 2.05 µm with 1 Hz frequency and uses a performance enhancing off-axis cavity ring down spectroscopy. Mole fraction of isotopic composition also depends on internal cavity pressure and temperature hence maintained constant at 119.14 Torr and 45.36 °C respectively (Mahesh et al., 2015). To keep the moisture as constant and as low as possible in the analyzer, sample and reference gases are passed through a Neflon drying unit. The dry mole fractions of CO_2 where the measured mole fraction of H_2O, which is also in ppm has been removed as shown in Equation 1.

$$CO_2(\text{ppm})_{\text{dry}} = \left(\frac{CO_2\ (\text{ppm})_{\text{wet}}}{(1 - \frac{H_2O\ (\text{ppm})}{10^6})} \right) \quad (1)$$

The ^{13}C-CO_2 and ^{18}O-CO_2 compositions are reported as $\delta^{13}C$ and $\delta^{18}O$ respectively versus VPDB (Vienna Pee Dee Belemnite) and reported in per mil (‰) as shown in Equation (2) and (3)

$$\delta^{13}C\ ((‰) = \left(\frac{C_s}{C_r} - 1\right) \times 1000 \quad (2)$$

$$\delta^{18}O\ ((‰) = \left(\frac{O_s}{O_r} - 1\right) \times 1000 \quad (3)$$

Where C_s, C_r, O_s, and O_r defined as follows; $C_{s\ (sample)} = (^{13}C/^{12}C)_s$; $C_{r\ (VPDB)} = (^{13}C/^{12}C)_r$; $O_{s\ (sample)} = (^{18}O/^{16}O)_s$ and $O_{r\ (VPDB)} = (^{18}O/^{16}O)_r$

2.2. Calibration of CO_2 isotope analyzer

The CO_2-CCIA-EP is calibrated using National Oceanic and Atmospheric Administration (NOAA) supplied CO_2 isotope calibration reference gases (ID: CC718409) towards eliminating instrument drifts and generating high quality data. The precision and accuracy of the instrument are computed by performing the internal calibration on 8th January 2020 with a 404.53±0.21 ppm of CO_2, -8.45±0.01 ‰, VPDB of $\delta^{13}C$ and -1.28±0.03 ‰, VPDB of $\delta^{18}O$ respectively. An inflow of reference gas has been passed through the Neflon drying unit for 15 minutes and collected data at 1 Hz frequency. Calibration is performed twice during the study period. Figure 2 shows the time series of CO_2, $\delta^{13}C$-CO_2 and $\delta^{18}O$-CO_2 during the calibration process. The shaded area in figure 2 represents ± 1 σ standard deviation.

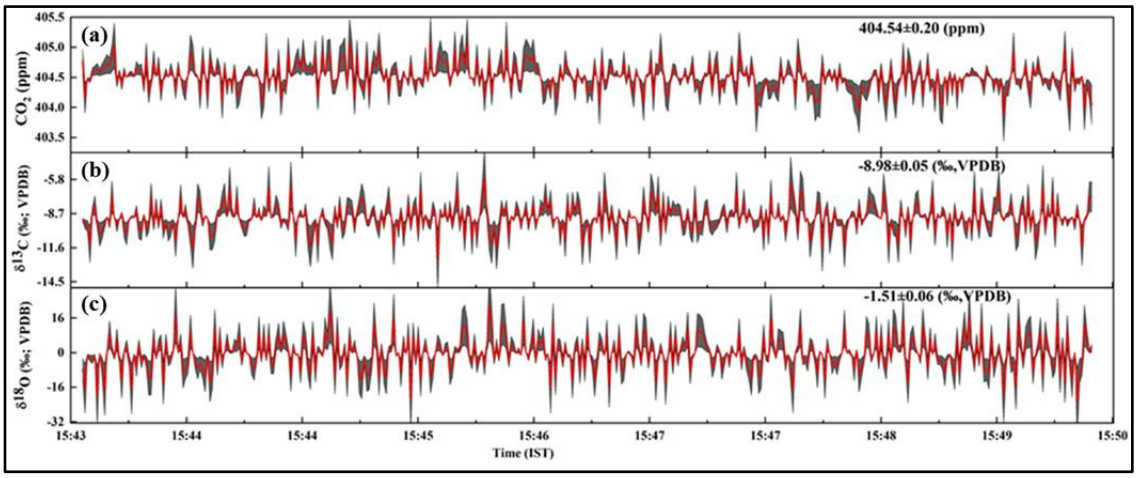

Figure 2. Time series of isotopic composition during the calibration process.

The 100 sec (1 σ) average precision of CO_2, $\delta^{13}C$-CO_2 and $\delta^{18}O$-CO_2 are 0.20 ppm, 0.05 ‰ and 0.06 ‰ respectively. The result of the calibration report is summarized in table 1.

Cylinder ID	$\frac{CO_2\ (ppm, ref) \pm 1\sigma}{CO_2\ (ppm, M) \pm 1\sigma}$	$\frac{\delta^{13}C\ of\ CO_2\ (‰, ref) \pm 1\sigma}{\delta^{13}C\ of\ CO_2\ (‰, M) \pm 1\sigma}$	$\frac{\delta^{18}O\ of\ CO_2\ (‰, ref) \pm 1\sigma}{\delta^{18}O\ of\ CO_2\ (‰, M) \pm 1\sigma}$
NOAA,CC718409	$\frac{404.53 \pm 0.21\ (ppm)}{404.54 \pm 0.20\ (ppm)^*}$	$\frac{-8.45 \pm 0.01\ (‰, VPDB)}{-8.98 \pm 0.05\ (‰, VPDB)^*}$	$\frac{-1.28 \pm 0.03\ (‰, VPDB)}{-1.51 \pm 0.06\ (‰, VPDB)^*}$
Bias (Ref-M)	-0.01 (ppm)	0.53 (‰)	0.23 (‰)
Precision	0.05%	0.55%	3.97%
Accuracy	$0.00\overline{247} = 0.01\%$	6.27%	17.96%
Ref: Reference; M: Measured		*Indicates 1σ calculation for 100sec average	

Table 1 Calibration report of CO_2, $\delta^{13}C$-CO_2 and $\delta^{18}O$-CO_2.

Bias between reference and measured values of CO_2, $\delta^{13}C$-CO_2 and $\delta^{18}O$-CO_2 are -0.01 ppm, 0.53 ‰ and 0.23 ‰ respectively. The precision and accuracy of CO_2, $\delta^{13}C$-CO_2 and $\delta^{18}O$-CO_2 are deduced with an averaging time of 100 sec. Results of the calibration in precision term are 0.05 %, 0.55 % and 3.97% for CO_2, $\delta^{13}C$-CO_2 and $\delta^{18}O$-CO_2 respectively. The precision of $\delta^{18}O$-CO_2 is coarse compared $\delta^{13}C$-CO_2, which may be improved by performing calibration for longer averaging time. However, one needs to compromise for the precision averaging time (Guillon et al., 2015). The second level quality was applied to the raw data by adjusting the respective biases.

2.3. Isotopic fraction using Improved model by Miller and Tans

With the calibrated CO_2, ^{13}C-CO_2 and ^{18}O-CO_2 data, implemented smoothing technique proposed by Thoning et al. (1989). This curve fitting function consist of a polynomial and harmonics terms, which accounts for short-term variability in the data. Subsequently, we computed biases (Δ) of CO_2, $\delta^{13}C$-CO_2 and $\delta^{18}O$-CO_2 respectively in order to calculate the isotopic signature as explained by Miller and Tans et al. (2003). Following equation is the improved model by Miller and Tans, which was implemented in the present study.

$$(\delta^{13}C \times CO_2)_{obs} - (\delta^{13}C \times CO_2)_{smooth} = \delta_s\left(CO_{2_{obs}} - CO_{2_{smooth}}\right) \quad (4)$$

δ_s, $CO_{2_{obs}}$ and $CO_{2_{smooth}}$ in equation (4) are slope representing multiple sources, observational CO_2 and smoothed CO_2 respectively. Further to obtain the slope between ΔCO_2 versus $\Delta(\delta^{13}C \times CO_2)$ and $\Delta(\delta^{18}O \times CO_2)$, ordinary least square (OLS) method was applied on day and night time hours during the study period. The OLS is more commonly known as linear regression which may be simple regression or multiple depending on number of explanatory variables. Generic model of the OLS is defined as shown in Equation (5).

$$y = a_0 + \sum_{i=1}^{n} \delta_i x_i + \epsilon \quad (5)$$

where y is $\Delta(\delta^{13}C \times CO_2)$, the dependent variable, a_0 is the intercept of the model, δ_i and x_i are the slope and ΔCO_2 corresponds to the i^{th} explanatory variable of the model (i = 1 to n), and ϵ is the random error. Similarly, equations 4 & 5 are implemented for computing the slope between ΔCO_2 versus $\Delta(\delta^{18}O \times CO_2)$. With these methods, further results are discussed in the following sections.

3.Results and Discussion

3.1. Seasonal Diurnal variation of CO_2, $\delta^{13}C$ and $\delta^{18}O$

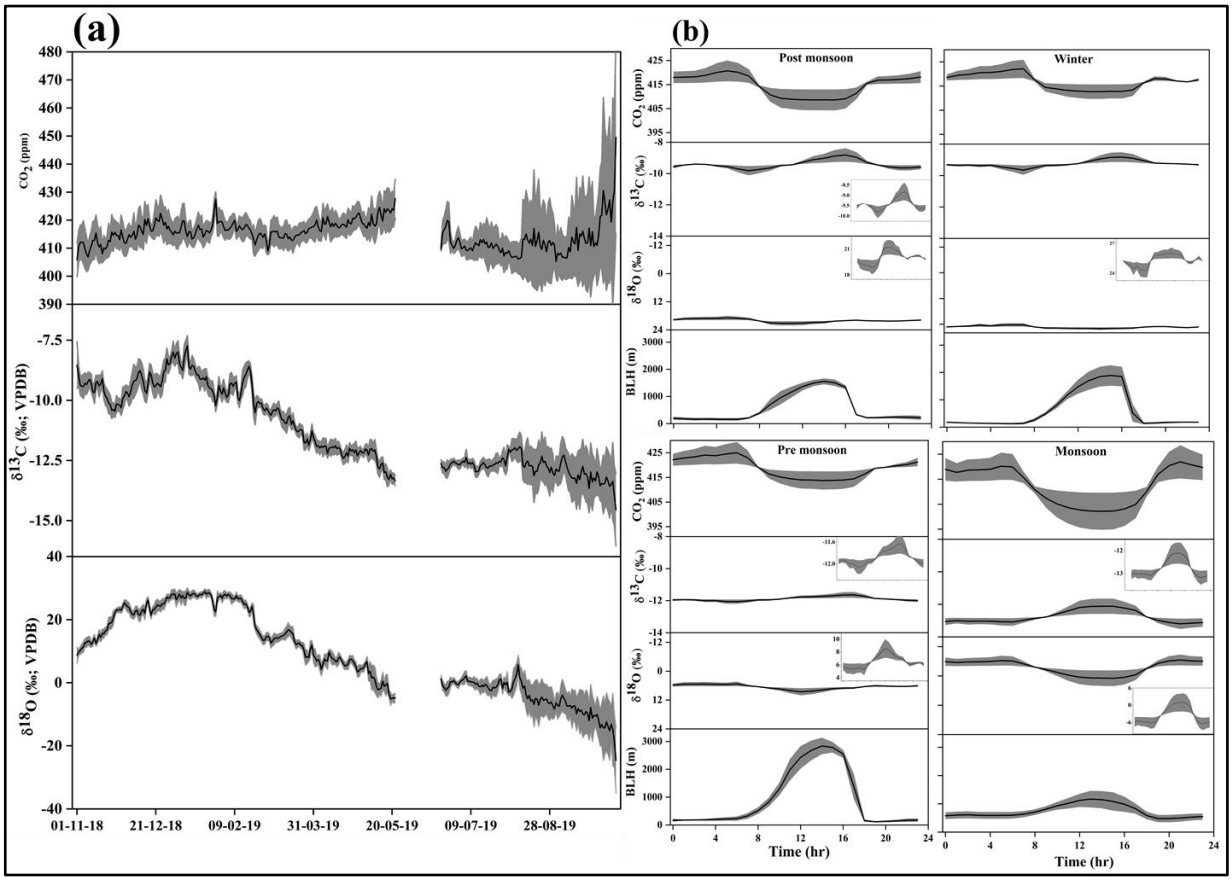

Figure 3. (a) Time series of (daily averaged) CO_2 (top), $\delta^{13}C$ (middle) and $\delta^{18}O$ (bottom). (b**)** Seasonal diurnal variations of CO_2, $\delta^{13}C$, $\delta^{18}O$ and boundary layer hight during the study period.

Global to regional carbon cycle can be understood in detail by using the stable isotopic composition of atmospheric CO_2 as a tracer. Hence, the present study is attempted to produce results of atmospheric CO_2 and its controlling factors in the sub-urban region of India using simultaneous stable isotopic measurements. The time series analysis as shown in figure 3a clearly depicts temporal variability in CO_2, ^{13}C-CO_2 and ^{18}O-CO_2 at the study site. Daily means of $\delta^{13}C$ and $\delta^{18}O$ show a clear decrease with an increase of atmospheric CO_2, which indicating the associated source-sink mechamisams. The data gaps in CO_2, $\delta^{13}C$ and $\delta^{18}O$ during 23rd May to 19th June, 2019 was due to instrument technical snag. During the study period, the atmospheric CO_2 concentration ranged from 405 ppm to 450 ppm, with its stable isotopic composition ranging from -7.72 to -14.55 ‰ VPDB for $\delta^{13}C$ and from -24.63 to 28.91 ‰ VPDB for $\delta^{18}O$ respectively. Moreover, larger standard devations in CO_2 and its stable isotopes are observed in October, 2019 indicating the large variability. This could be due to varied sources namely change in surface emissions, seasonal biomass burnig and long-range influence along with the reversal of monsoonal winds (north-east) at the study site. However, found smaller variability in CO_2 and its stable isotopes during Indian summer monsoon (ISM, June-July-August-September) indicating marine fluxes (Tiwari et al., 2014) besides local sources.

The study site experience 4 seasons namely post-monsoon (November-December, vegetation-II), winter (January-February), pre-monsoon (March-May, also known as summer months-dry season) and summer monsoon (June-September; vegetation-I). Thus, figure 3b shows diurnal variations of seasonal CO_2, $\delta^{13}C$ and $\delta^{18}O$ against BLH. The height of the Boundary Layer is the vertical extent of air column driven by convection processes associated with the earth's surface heating (Stull, 1988). Due to strong convection and associated surface temperature, the BLH attains maximum height in the afternoon, which modulates the dispersion of air pollutats in the mixed layer. In contrast to this, the BLH quickly collapses and reaches stable form during night hours due to the absence of convection processes. BLH is maximum (minimum) during pre-monsoon (summer monsoon) with 2839 m (1167 m) respectively, which indicates strong convection in the dry season. Subsequently, observed low (high) CO_2 concentration during strong (absence) convective hours. The maximal seasonal variation in CO_2 is found during pre-monsoon with a mean value of 418.88 ± 4.07 ppm. The strong afternoon drop of CO_2 during pre-monsoon is associated with the peak BLH of 2839 m. In contrast, minimum seasonal variation in CO_2 is found during summer monsoon due to low BLH (1167 m). Thus, exhibits prominent diurnal variations of CO_2 and $\delta^{13}C$ against BLH during all the seasons which is also attributed to isotopic fractionation processes during biological activity (Demény and Haszpra 2002). Except for monsoon, diminished diurnal seasonal variability observed with $\delta^{18}O$ (Murayama et al., 2010) compared to CO_2 and $\delta^{13}C$ at present study site. Besides the influence of BLH, minimum CO_2 and maximum $\delta^{13}C$ and $\delta^{18}O$ during afternoon hours are due to the uptake of CO_2 by the plants through photosynthesis process. During night hours, the concentration CO_2 is maximum with low $\delta^{13}C$ and $\delta^{18}O$ due to active terrestrial respiration (Sreenivas et al., 2016). Therefore, seasonal diurnal patterns of CO_2 and $\delta^{13}C$ are anti-correlated during all the seasons with minimum CO_2 in daytime and maximum $\delta^{13}C$ respectively (figure 3b). Similarly, Pang et al. (2016) observed a negative relationship of $\delta^{13}C$ diurnal cycle with CO_2 mixing ratio at Beijing, in Northern China.

Seasonal averages of CO_2 ($\delta^{13}C$ & $\delta^{18}O$) during post-monsoon, winter, pre-monsoon and summer monsoon are 414.70±4.49 ppm (-9.41±0.27 ‰ & 20.03±0.73 ‰), 416.84±3.25 ppm (-9.25±0.21 ‰, & 25.95±0.57 ‰), 418.88±4.07 ppm (-11.88±0.13 ‰ & 6.51±0.98 ‰), 412.61±7.59 ppm (-12.76±0.38 ‰ & -3.49±2.87 ‰) respectively. Site specific $\delta^{13}C$ seasonal values with other study sites in India and across the world are summarized in table 2. Liu et al. (2014a) showed annual means of $\delta^{13}C$ varying from -8.30 ‰ to -8.35 ‰ at Waliguan station in China. Further, the annual means of $\delta^{13}C$ are -8.27 ‰ and -8.36 ‰ respectively for 2009 and 2010 at Shangdianzi station which is located in a small village about 100 km northeast of Beijing (second populated urban city in China). This site is influenced by strong pollution events from Beijing and surrounding urban areas in the presence of southwesterly winds. Also, the annual mean of $\delta^{13}C$ were -8.55‰, -8.52%, -8.46% and -8.61% during 2007-2010 at Tae-ahn Peninsula which is located on a small Peninsula on the western coast of Korea. Irrespective of the sites background influence, results of worldwide sites mentioned above indicates $\delta^{13}C$ values are in close proximity with our present observations.

An increase and decrease of $^{18}O/^{16}O$ ($\delta^{18}O$) ratio of CO_2 in the atmosphere across the seasons indicates dominance of photosynthesis and ecosystem respiration. During the study period, the atmospheric $\delta^{18}O$–CO_2 varies seasonally from -3.49 ‰ to + 25.95 ‰ with large scatter compared to seasonal CO_2 and $\delta^{13}C$. The scatter could be due to vegetation cover, leaf water content, retention of soil water and ocean (Zhou et al., 2006). However, interpretation of

seasonal $\delta^{18}O$ is not that straight as CO_2 and $\delta^{13}C$ due to the varying fluxes of biospheric CO_2 and prevailing meteorology at the study site.

High atmospheric CO_2 in pre-monsoon followed by winter and subsequent increase of $\delta^{18}O$-CO_2 in the atmosphere in the absence of relatively low photosynthesis could be attributed to long-range air mass transport with enhanced $\delta^{18}O$-CO_2 and fossil fuel burning activities (Murayama et al., 2010). Through isotopic exchange, $\delta^{18}O$-CO_2 in the atmosphere may affect due to variation in the ^{18}O from precipitation and soil respiration (Kato et al., 2004). Newman et al. (2008) observed the range of $\delta^{18}O$ at Los Angeles basin, Southern California during 1972 -1973 (1998-2003) is -3.56 ‰ to + 0.21 ‰ (-3.99 ‰ to +0.45 ‰) and average value during 1972-1973 (1998-2003) of $\delta^{18}O$ is -1.28 ‰ (-1.07‰).

Study sites	$\delta^{13}C$ values (‰) Seasonal	References
Dallas, USA	-12.0 to -8.1	Clark-Thorne and Yapp, 2003
Bern, Switzerland	-14 to -8	Sturm et al.,2006
Salt Lake City, USA	-18 to -8 (December 2004 - January 2005)	Pataki et al., 2006
Los Angeles, USA	-9.3 to -7.5 (Oct) -12.5 to -8.8 (Dec) -12.2 to -9.2 (Feb) -12.5 to -10.2 (April)	Djuricin et al., 2010
Nagoya, Japan	-13.4 to -8.5(May) -15.0 to -8.5 (December from 2008 - 2009)	Wada et al., 2011
Krakow, Poland	-11 to -9.5	Zimnoch et al., 2004
Wroclaw (SW Poland)	-16.4 to -8.2	Gorka et al., 2013
Cabo de Rama (West Coast of India)	-8.4 to -7.8	Bhattacharya et al., 2009
NRSC, Shadnagar, India	-9.3 to -12.8 (November 2018 - October 2019)	Present study

Table 2 $\delta^{13}C$ values from different study sites.

Seasonal amplitude (peak to peak ±1 SD) of atmospheric CO_2 was 9.82 ± 1.39 ppm, 7.19 ± 0.11 ppm, 9.23 ±2.1 ppm and 17.30 ± 9.29 ppm in post-monsoon, winter, pre-monsoon and summer monsoon respectively. Weak and strong seasonality was observed during winter and monsoon seasons repectively reflecting enrichment of atmospheric CO_2 in low vegetation months and depleting CO_2 in high vegetation season. The NDVI in figure 1b show maximum during monsoon and minimum during rest of the seasons. The Sinhagad and Cape Rama, two marine stations of western India showed CO_2 seasonal amplitudes between 8-10 ppm during monsoon and >15ppm for remaining seasons (Tiwari et al., 2014), which could be due to the influence of land-sea breeze (Mahesh et al., 2014). The seasonal amplitude of $\delta^{13}C$ ($\delta^{18}O$) are 0.48 ± 0.06 ‰ (1.91 ± 0.005 ‰), 0.44 ± 0.02 ‰ (1.60 ± 0.13 ‰), 0.32 ± 0.09 ‰ (2.53 ± 1.003 ‰) and 0.87 ± 0.73 ‰ (6.58 ± 4.10 ‰) in post-monsoon, winter, pre-monsoon and summer monsoon respectively. Thus, modulation in the seasonal amplitude of CO_2 in the atmosphere is attributed to the rate of photosynthesis and respiration besides the impact of local and long-range prevailing meteorology. For better understanding of the relationship between atmospheric CO_2 against its

stable isotopic composition, improved model by Miller and Tans was adopted by fitting linear regression using the OLS.

3.2. Seasonal correlation between CO_2, $\delta^{13}C$ and $\delta^{18}O$ using the improved model by Miller and Tans

Since the study site is not a single sourced location and is in proximity of Hyderabad city , a metropolitan city of India, the Miller-Tans (2003) method was applied on the day and night time observations to characterize the effective $\delta^{13}C$ ($^{13}C/^{12}C$) source ratios at the study site. In order to estimate the slope (δ_s) for $\delta^{13}C$ and $\delta^{18}O$, the ordinary least square curve fitting was applied to ΔCO_2 against $\Delta(CO_2 \times \delta^{13}C)$ and $\Delta(CO_2 \times \delta^{18}O)$ respectively and results shown in Figure 4(a-b). The improved model by Miller and Tans is applied to capture the processes of day and night which are driving the atmospheric CO_2. During the day (night) time $\delta^{13}C$ slopes in post-monsoon, winter, pre-monsoon and monsoon are -10.43 ± 5.60 ‰ (-27.08 ± 4.21 ‰), -36.43 ± 8.11 ‰ (-25.11 ± 5.55 ‰), -32.02±4.57 ‰ (-23.79 ± 2.08 ‰) and -52.50±4.60 ‰ (-28.38 ± 1.29 ‰) respectively with coefficient of determination (R^2) ranging from 0.06 (0.26) in post-monsoon (winter) to 0.56 (0.83) in monsoon. The strong correlation in summer-monsoon during day and night time can be attributed to the long-range air mass sources transported by the monsoonal winds and sinks may be attributed to the terrestrial biospheric activites at the study site. The $\delta^{13}C$ slope during daytime is largely varied in all the seasons representing the contribution of mixed source emissions at the regional scale and suppressed local sources (Xu et al., 2017). An average value of daytime δ_s of $\delta^{13}C$ during all seasons is -32.84 ‰ indicating the source of atmospheric CO_2 is related to gasoline and natural gas combustion in and around the study site (Clark-Thorne and Yapp, 2003). The estimated slopes are evaluated statistically and found significant (p-value < 0.05) with 95 % confidence interval during all the seasons. The $\delta^{13}C$ slopes in night time during all the seasons are between -23.79 ‰ to -28.38 ‰, with an average value of -26.09 ‰. In general, the average value of δ_s of $\delta^{13}C$-CO_2 is -26.20 ‰ for C_3 ecosystem respiration (Pataki et al., 2003). Thus, the present study also confirm the dominance of C_3 vegetation at the study site contributes to the emissions of atmospheric CO_2 mixing ratio during night time. The varied δ_s of $\delta^{13}C$-CO_2 in different study locations are attributed to the the local anthropogenic activities and terrestrial biospheric pathways.

As shown in figure 4b, improved model by Miller and Tans was implemented on $\delta^{18}O$ by substituting for $\delta^{13}C$ in equation 4 to see the relationship between $\delta^{18}O$ and CO_2 concentration. Figure 4b show strong correlation of $\delta^{18}O$ with $R^2 = 0.75$ in night hours of monsoon. During the same period, $\delta^{13}C$ is also strongly correlated with CO_2 concentration, indicating the active role of biospheric – atmospheric interactions in the exchange of CO_2. In contrast, varied seasonal slopes of $\delta^{13}C$ and $\delta^{18}O$ were observed in daytime representing the study site is also dominated by the regional sources via upwind transport along with the influence of local terrestrial activities namely boundary layer dynamics and photosynthesis. During daytime, the δ_s of $\delta^{18}O$ shows scatter across the seasons for which the driving forces are different (Yakir et al., 2011). With the present study, we understand that interpretation of the seasonal $\delta^{18}O$ variation is complicated compared to $\delta^{13}C$ and CO_2 mixing ratio. However, current knowledge on $\delta^{18}O$ seasonality can be improved with great understanding of varying fluxes of bisopheric CO_2 and role of prevailing meteorology at the study site.

The δ_s of $\delta^{13}C$ and $\delta^{18}O$ analysis at the study site confirms the prominence of C_3 ecosystem activities viz. photosynthesis and respiration in the variability of atmospheric CO_2 during vegetative seasons. During dry seasons (winter and pre-monsoon), the δ_s values indicates the important role of local and long-range combustion processes that enrich atmospheric CO_2 at the study site. However, this information is pertained to the total source contributions and individual source apportionment was not carried out in this study.

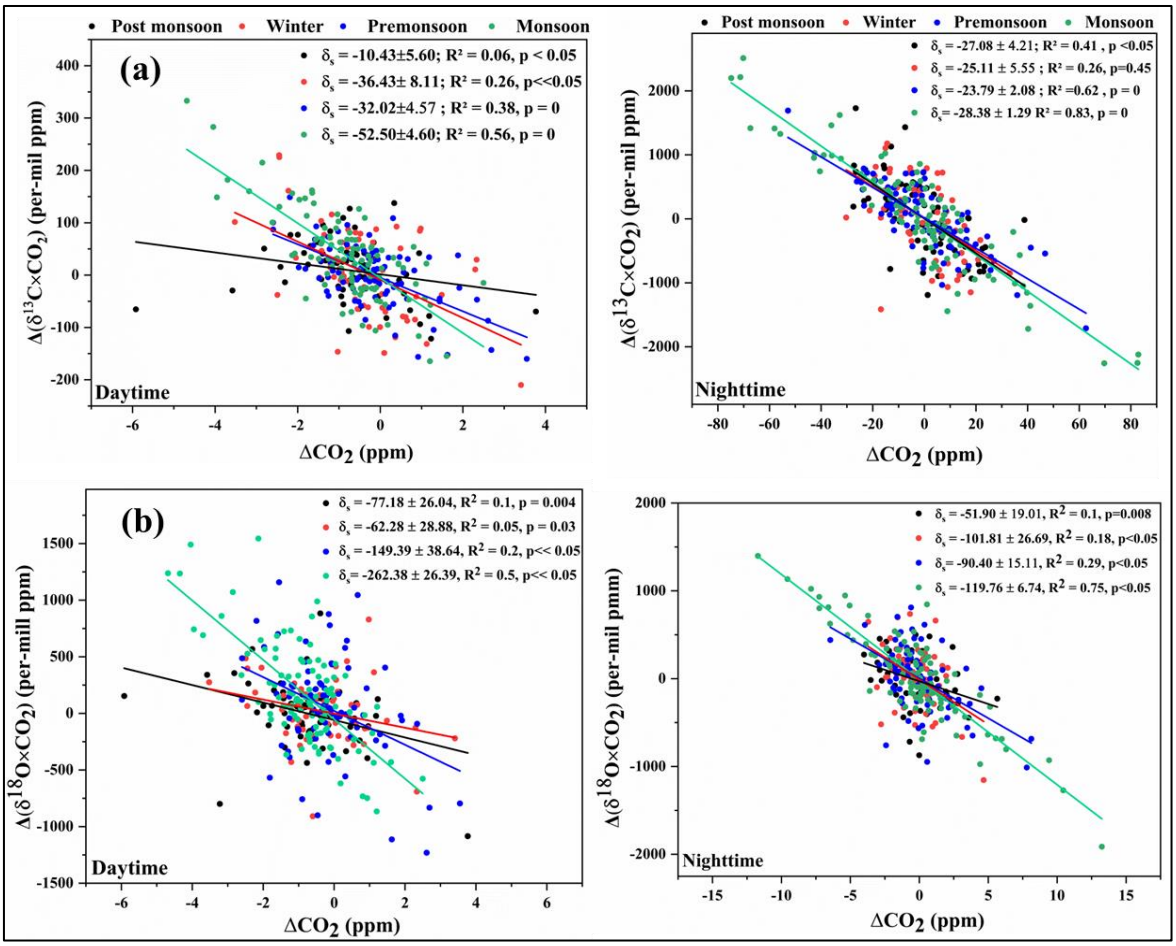

Figure 4. Improved Miller and Tans method applied to the (a) Seasonal ΔCO_2 vs $\Delta(CO_2 \times \delta^{13}C)$ during day (Top left panel) and nighttime (Top right panel) hours (b) Bottom left panel shows ΔCO_2 vs $\Delta(CO_2 \times \delta^{18}O)$ during daytime and bottom right panel shows nighttime. The solid line represents the regression fit using ordinary least square method.

488

Month	**Daytime** ΔCO_2 vs Δ ($CO_2 \times \delta^{13}C$) [ΔCO_2 vs Δ ($CO_2 \times \delta^{18}O$)]		**Nighttime** ΔCO_2 vs Δ ($CO_2 \times \delta^{13}C$) [ΔCO_2 vs Δ ($CO_2 \times \delta^{18}O$)]	
	'r'	Slope	'r'	Slope
November, 2018	-0.49 [-0.12]	-18.30 [-23.18]	-0.75[-0.21]	-29.90[-26.40]
December, 2018	-0.52 [-0.57]	-42.30 [-132.37]	-0.56[+0.25]	-24.72[+26.38]
January, 2019	-0.56 [-0.46]	-33.12 [-98.68]	-0.63[-0.80]	-24.18[-176.55]
February, 2019	+0.40 [+0.09]	+28.83 [+22.94]	-0.41[+0.21]	-27.01[+49.61]
March, 2019	-0.49 [-0.14]	-28.51 [-79.64]	-0.66[-0.33]	-18.72[-65.29]
April, 2019	-0.65 [-0.33]	-33.94 [-92.92]	-0.84[-0.44]	-26.10[-77.5]
May, 2019	-0.84 [-0.51]	-37.58 [-200.60]	-0.81[-0.72]	-24.91[-103.5]
June, 2019	-0.15 [-0.87]	-11.31 [-279.45]	-0.95[-0.96]	-24.25[-113.25]
July, 2019	-0.40 [-0.51]	-24.25 [-182.29]	-0.63[-0.71]	-26.29[-126.12]
August, 2019	-0.71 [-0.55]	-52.01 [-239.16]	-0.93[-0.89]	-29.29[-122.94]
September, 2019	-0.94 [-0.79]	-72.46 [-287.80]	-0.93[-0.87]	-28.36[-118.20]
October, 2019	-0.95 [-0.95]	-51.23 [-227.49]	-0.99[-1.0]	-27.39[-140.52]

489 **Table 3** Monthly correlation coefficient (r), and slope (δ_s) derived from the improved Miller and
490 Tans method

491 Table 3 shows monthly 'r' and slope values derived between ΔCO_2 vs Δ ($CO_2 \times \delta^{13}C$) and ΔCO_2
492 vs Δ ($CO_2 \times \delta^{18}O$) during day and night hours respectively. The average monthly value of $\delta^{13}C$
493 slope during night time (daytime) is -26 ‰ (36.15‰). During nighttime the average value of
494 slope at the study site is close to C_3 ecosystem respiration and during day time the average value
495 of slope is close to sources which are combustion, photosynthesis processes and long range
496 transport. The differences in slope value at various study sites is due to photosynthesis pathways
497 and local anthropogenic sources prevailing at the study areas (Pang et al., 2016). In similar
498 studies carried by various authors slope values at their study site is as follows. Liu et al. (2014a)
499 observed annual mean value of slope which is -25.44‰ and -21.70‰ at Waliguan and
500 Shangdianzi stations in China respectively. Zhou et al. (2006) studied the isotopic fractionation
501 at 12 stations of Northern Hemisphere and found slope (δ_s) ranging from -28.85‰ to - 26.50‰
502 with improved Miller-Tans method. Murayama et al. (2010) observed δ_s value of -28.7‰
503 averaged over the study period at Takayama site in central Japan which is also comparable to the
504 present study site. The δ_s of $\delta^{18}O$ during vegetation - I and II periods is strongly correlated (r >
505 0.7) compared to 'r' value during other months. Thus, vegetation cover is an important
506 component in variability of $\delta^{18}O$ of atmospheric CO_2.
507 The correlation coefficient (r) between $\delta^{18}O$ and $\delta^{13}C$ during daytime (night time) are
508 0.13 (0.07), 0.64 (0.60), 0.95 (0.93), 0.24 (0.92) for post-monsoon, winter, pre-monsoon and
509 summer monsoon seasons respectively. A very strong positive correlation (0.93 to 0.95) in day
510 and night hours during pre-monsoon between $\delta^{18}O$ and $\delta^{13}C$ might be due to high vapour
511 pressure deficit (VPD) than the post monsoon (low VPD). The high VPD and summer conditions
512 are supportive for high transpiration as well as photosynthetic activities as sunshine hours are
513 more during pre-monsoon than post monsoon (approaching towards winter). Low $\delta^{13}C$ and $\delta^{18}O$
514 correlation during post-monsoon indicates high stomatal conductance in vegetation, ensuring
515 enhanced release of water to the atmosphere (Cullen et al., 2008; Liu et al., 2014b). Our study

showed clear evidence of an increase or decrease of atmospheric CO_2 is associated with the changes of its isotopic composition during photosynthesis and biogenic respiration besides local and long-range anthropogenic influences. Also, Zimnoch et al. (2004) observed good correlation between $\delta^{18}O$ and $\delta^{13}C$ with 'r' ranging from 0.84 to 0.94 in their observations while studying their diurnal variability from Poland. Further to understand the influence of transport pathways on atmospheric CO_2 via long range air mass is examined in the present study using Hybrid Single Particle Lagrangian Integrated Trajectory (HYSPLIT, https://www.ready.noaa.gov/HYSPLIT.php) Model.

3.3. Influence of local and long-range airmass on atmospheric CO_2

Study site being a sub-urban region and about 60 km away from the Hyderabad city, the analysis of improved Miller-Tan model depicts atmospheric CO_2 concentration at the study site is mainly controlled by terrestrial biosphere activities during the study period. During the day hours, the derived δ_s of $\delta^{13}C$ indicating mixed source contribution at the study site, which may be possibly due to combustion activities, biomass burning and the transportation of air mass. Seasonal wind vector obtained from the ECMWF at 850 hPa over the Indian region are shown in figure 5a. The long-range air mass circulation that is reaching the study site has been analyzed using Lagrangian back-trajectory model along with the fire counts during all the seasons (Figure 5b).

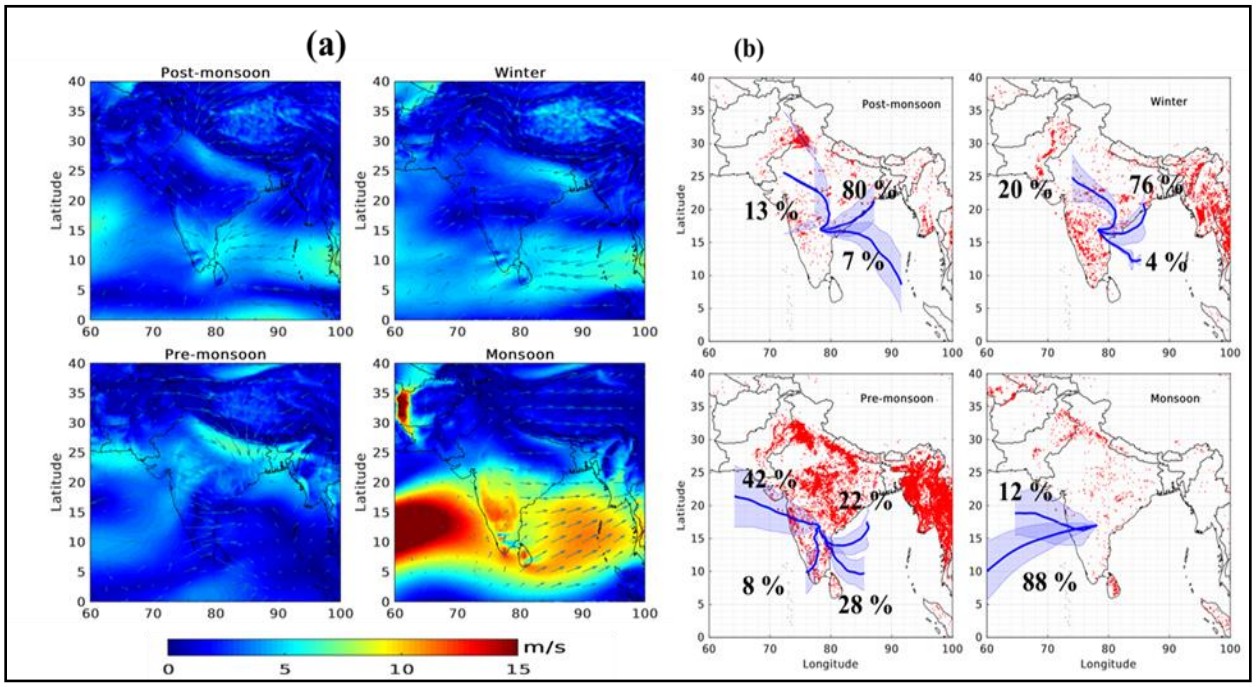

Figure 5. (a) Mean winds (m s^{-1}) at 850 hPa (b) Seasonal long-range air mass circulation at 2 km altitude using HYSPLIT

During the Indian summer-monsoon season, predominantly the south- westerly (SW) winds are present as shown in figure 5a, which brings maritime air mass (Bhattacharya et al., 2009; Tiwari et al., 2014) over the Indian region. The atmospheric CO_2 concentration at the study site is observed minimum during the summer-monsoon period indicating the contribution of monsoon

circulation through scavenging effect (Tiwari et al., 2014; Mahesh et al., 2014). The maritime air mass during summer-monsoon is relatively pristine due to the absence of anthropogenic sources thus observed low atmospheric CO_2 concentration at the study site.

A Lagrangian back trajectory analysis as shown in figure 5b also confirms the observed low atmospheric CO_2 due to influence of maritime air mass (88 %) during the summer-monsoon period. During winter and pre-monsoon, enrichment of atmospheric CO_2 at the study site could be due to the predominant continental sources reaching from the north-east (NE, 76 %) and north-west (NW, 42 %) respectively. Figure 5b shows seasonal long-range air mass circulation over laid with fire count obtained from Moderate Resolution Imaging Spectroradiometer (MODIS) during the study period. During pre-monsoon and post-monsoon, agriculture residue burning is commonly observed in Punjab, Haryana and Indo Gangetic Plains (IGBP) areas of India (Liu et al., 2019), which are in NW and NE directions of the study site. Thus, the present study reveals that during these seasons, the biomass burning is one of continental sources contributing to the elevated CO_2 concentration. Therefore the variability of atmospheric CO_2 concentration at the study site is greatly influenced by the maritime air mass during summer-monsoon and continental sources during other seasons.

4. Conclusion

The present study examined the diurnal and seasonal variations of atmospheric CO_2 and its stable isotopes $\delta^{13}C$ and $\delta^{18}O$ at the sub-urban site of Telangana, India during November 2018 to October 2019 using high precision CO_2 isotopic analyzer.

Following are the salient findings of the present study

1. The atmospheric CO_2 concentration ranged from 405 ppm to 450 ppm, with its stable isotopic composition ranging from -7.72 to -14.55 ‰ VPDB for $\delta^{13}C$ and from -24.63 to 28.91 ‰ VPDB for $\delta^{18}O$ respectively.
2. The CO_2 and $\delta^{13}C$ exhibit clear diurnal variation with opposite patterns during all the seasons with minimum CO_2 and maximum $\delta^{13}C$ in daytime and vice versa.
3. During strong convective hours (peak BLH), observed low atmospheric CO_2 concentration and high CO_2 concentration in weak convection period indicating strong atmospheric mixing due to the convective boundary layer.
4. Seasonal amplitude (peak to peak ±1 SD) of atmospheric CO_2 at the study site was 9.82 ± 1.39 ppm, 7.19 ± 0.11 ppm, 9.23 ±2.1 ppm and 17.30 ± 9.29 ppm in post-monsoon, winter, pre-monsoon and summer monsoon respectively. Large seasonality in summer-monsoon at the study site due to strong influence of monsoonal winds, precipitation and vegetation cover.
5. To capture the driving processes of atmospheric CO_2 during day and night hours, we thus applied improved Miller-Tans model on seasonal ΔCO_2, Δ ($CO_2 \times \delta^{13}C$) and Δ ($CO_2 \times \delta^{18}O$) data. During all seasons, mean δ_s of $\delta^{13}C$ value is -32.84 ‰ in daytime indicating the source of atmospheric CO_2 is related to gasoline and natural gas combustion at the study site and nighttime δ_s values were between -23.79 ‰ to -28.38 ‰, with an average value of -26.09 ‰ representing the dominance of C_3 ecosystem respiration.

6. Seasonal 'r' value between $\delta^{18}O$ and $\delta^{13}C$ during day and night time varied from 0.13 to 0.95 and 0.07 to 0.93 respectively. A very strong positive correlation (0.93 to 0.95) in day and night hours during pre-monsoon between $\delta^{18}O$ and $\delta^{13}C$ might be due to high VPD than the post monsoon (low VPD).
7. Upwind transport confirms the influence of biomass burning on enriched atmospheric CO_2 during pre-monsson and post-monsoon seasons.
8. A lagrangian back-trajectories confirms the variability of atmospheric CO_2 concentration at the study site is largely influenced by the maritime airmass during summer-monsoon and continental sources in other seasons.

Our study showed clear evidence of an increase or decrease of atmospheric CO_2 is associated with the changes of its isotopic composition during photosynthesis and biogenic respiration besides local and long-range anthropogenic influences. The variability in atmospheric CO_2 during monsoon season is strongly associated with the ISM. However, the individual source apportionment of different sources is not discussed in this present study.

Acknowledgements

Authors sincerely thank Dr Raj Kumar, Director NRSC for his kind encouragement and support to carry out this work. This work was part of the Atmospheric CO_2 Retrievals and Monitoring (ACRM) of the National Carbon Project (NCP) funded by CAP-IGBP. Authors thank Dr. M.V.R Sesha Sai, Deputy Director, ECSA for his encouragement to carry this study. We also thank Dr. V.K Dadhwal, Director, Indian Institute of Space Science and Technology, Trivandrum, India for reviewing the manuscript. We greatly acknowledge the HYSPLIT, ECMWF-ERA and MODIS fire teams for providing the scientific data sets used in this study. Authors also greatly acknowledge Bhuvan site for providing NDVI data which is derived from Oceansat-2 Ocean color monitor sensor.

Declaration of competing interest

The authors declare no competing interests.

Data Availabilty Statement

The *in- situ* data may be available publicly once archival is completed.

References

Andres, R.J., Marland, G., Fung, I., & Matthews, E. (1996). A 1°× 1° distribution of carbon dioxide emissions from fossil fuel consumption and cement manufacture, 1950–1990. *Global Biogeochem Cycles*, 10(3), 419-429. https://doi.org/10.1029/96GB01523.

Baer, D. S., Paul, J. B., Gupta, M., & O'Keefe, A. (2002). In Diode Lasers and Applications in Atmospheric Sensing; Fried, A., Ed. In SPIE-The International Society for Optical Engineering: Bellingham, WA, Vol. 4817, pp. 167-176.

Ballantyne, A.P., Alden, C.B., Miller, J.B., Tans, P.P., & White, J.W.C. (2012). Increase in observed net carbon dioxide uptake by land and oceans during the past 50 years. *Nature*, 488, 70-72, doi:10.1038/nature11299.

Bhattacharya, S.K., Borole, D.V., Francey, R.J., Allison, C.E., Steele, L.P., Krummel, P., et al. (2009). Trace gases and CO_2 isotope records from Cabo de Rama, India. *Current Science* 97(9), 1336-1344.

Cullen, L. E., Adams, M. A., Anderson, M. J., & Grierson, P. F. (2008). Analyses of $\delta^{13}C$ and $\delta^{18}O$ in tree rings of Callitris columellaris provide evidence of a change in stomatal control of photosynthesis in response to regional changes in climate. Tree Physiology, 28(10), 1525-1533. DOI: 10.1093/treephys/28.10.1525.

Clark-Thorne, S. T., & Yapp, C. J. (2003). Stable carbon isotope constraints on mixing and mass balance of CO2 in an urban atmosphere: Dallas metropolitan area, Texas, USA. Applied Geochemistry, 18(1), 75-95.

Djuricin, S., Pataki, D.E., & Xu, X. (2010). A comparison of tracer methods for quantifying CO_2 sources in an urban region. *Journal of Geophysical Research: Atomspheres* 115, 1–13, https://doi.org/10.1029/2009JD012236.

Demény A, Haszpra L (2002) Stable isotope compositions of CO_2 in background air and at polluted sites in Hungary. Rapid Commun Mass Spectrom 16:797–804

Farquhar, G. D., Lloyd, J., Taylor, J.A., Flanagan, L.B., Syvertsen, J. P., et al. (1993). Vegetation effects on the isotope composition of oxygen in atmospheric CO_2. *Nature*, 363(6428), 439-443, doi: 10.1038/365368b0

Francey, R. J., & Tans, P. P. (1987). Latitudinal variation in oxygen-18 of atmospheric CO_2. Nature, 327(6122), 495-497.

Górka, M., & Lewicka-Szczebak, D. (2013). One-year spatial and temporal monitoring of concentration and carbon isotopic composition of atmospheric CO_2 in a Wrocław (SW Poland) city area. *Applied geochemistry*, 35, 7-13. https://doi.org/10.1016/j.apgeochem.2013.05.010.

Guillon, S., Agrinier, P., & Pili, E., (2015). Monitoring CO_2 concentration and $\delta^{13}C$ in an underground cavity using a commercial isotope ratio infrared spectrometer. *Applied Physics B-Lasers and optics*, 119(1), 165-175. doi: 10.1007/s00340-015-6013-4.

675 Guha T, Ghosh P (2010) Diurnal variation of atmospheric CO_2 concentration and $\delta^{13}C$ in an
676 urban atmosphere during winter—role of the Nocturnal Boundary Layer. J Atmos Chem 65:1–
677 12. doi:10.1007/s10874-010-9178-6
678
679 Guha, T. and Ghosh, P. (2015). Diurnal and seasonal variation of mixing ratio and δ 13 C of air
680 CO_2 observed at an urban station Bangalore, India. Environmental Science and Pollution
681 Research, 22(3), 1877-1890. https://doi.org/10.1007/s11356-014-3530-3.
682
683 Huang, J., Yu, H., Guan, X., Wang, G., & Guo, R., (2016). Accelerated dryland expansion under
684 climate change, *Nature Climate Change*, 6, 166–171, http://dx.doi.org/10.1038/nclimate2837.
685
686 Kato, T., Nakazawa, T., Aoki, S., Sugawara, S., & Ishizawa, M. (2004). Seasonal variation of the
687 oxygen isotopic ratio of atmospheric carbon dioxide in a temperate forest, Japan. *Global*
688 *Biogeochem Cycles*, 18(2), https://doi.org/10.1029/2003GB002173.
689
690 Liu, L., Zhou, L., Vaughn, B., Miller, J. B., Brand, W. A., Rothe, M., & Xia, L. (2014a).
691 Background variations of atmospheric CO_2 and carbon-stable isotopes at Waliguan and
692 Shangdianzi stations in China. *Journal of Geophysical Research: Atmospheres*, 119(9), 5602-
693 5612.
694
695 Liu, X., An, W., Leavitt, S. W., Wang, W., Xu, G., Zeng, X., & Qin, D. (2014b). Recent
696 strengthening of correlations between tree-ring $\delta^{13}C$ and $\delta^{18}O$ in mesic western China:
697 Implications to climatic reconstruction and physiological responses. *Global and Planetary*
698 *Change*, *113*, 23-33.http://dx.doi.org/10.1016/j.gloplacha.2013.12.005.
699
700 Liu, T., Marlier, M. E., Karambelas, A., Jain, M., Singh, S., Singh, M. K., Gautam, R., &
701 DeFries, R.S. (2019). Missing emissions from post-monsoon agricultural fires in northwestern
702 India: regional limitations of MODIS burned area and active fire products. *Environmental*
703 *Research Communications* 1(1), 011007, https://doi.org/10.1088/2515-7620/ab056c.
704
705 Machida, T., Kita, K., Kondo, Y., Blake, D., Kawakami, S., Inoue, G., & Ogawa, T. (2002).
706 Vertical and meridional distributions of the atmospheric CO_2 mixing ratio between northern
707 midlatitudes and southern subtropics. *Journal of Geophyical Research: Atmospheres* 107(D3),
708 BIB 5-1-BIB 5-9, https://doi.org/10.1029/2001JD000910.
709

710 Mahesh, P., Sharma, N., Dadhwal, V. K., Rao, P. V. N., Apparao, B. V., Ghosh, A. K., & Ali,
711 M. M. (2014). Impact of land-sea breeze and rainfall on CO2 variations at a coastal station.
712 Journal of Earth Science & Climatic Change, 5(6), 1.

713 Mahesh, P., Sreenivas, G., Rao, P. V. N., Dadhwal, V. K., Sai Krishna, S. V. S., & Mallikarjun,
714 K. (2015). High-precision surface-level CO_2 and CH_4 using off-axis integrated cavity output
715 spectroscopy (OA-ICOS) over Shadnagar, India. *International Journal of Remote Sensing*
716 ,36(22), 5754-5765, https://doi.org/10.1080/01431161.2015.1104744.

Mahesh, P., Sreenivas, G., Rao, P. V. N., & Dadhwal, V. K. (2016). Atmospheric CO_2 retrieval from ground based FTIR spectrometer over Shadnagar, India. *Atmospheric Measurement Techniques Discussions,* https://doi.org/10.5194/amt-2016-177, 2016.

Mahalakshmi, D.V., Sujatha, P., Naidu , CV., Chowdary, V.M., (2014). Contribution of vehicular emissions on urban air quality: results from public strike in Hyderabad. Indian Journal of Radio & Space Physics (IJRSP), 43(6), 340-348.

Miller JB and Tans PP (2003) Calculating isotopic fractionation from atmospheric measurements at various scales. Tellus Series B: Chemical and Physical Meteorology 55: 207–214.

Monastersky, R. (2013). Global carbon dioxide levels near worrisome milestone. *Nature*, 497 (7447), 13–14, https://doi.org/10.1038/497013a.

Murayama, S., C. Takamura, S. Yamamoto, N. Saigusa, S. Morimoto, H. Kondo, T. Nakazawa, S. Aoki, T. Usami, and M. Kondo (2010), Seasonal variations of atmospheric CO_2, $\delta^{13}C$, and $\delta^{18}O$ at a cool temperate deciduous forest in Japan: Influence of Asian monsoon, J. Geophys. Res., 115, D17304, doi:10.1029/2009JD013626.

Nalini, K., Sijikumar, S., Valsala, V., Tiwari, Y. K., & Ramachandran, R. (2019). Designing surface CO_2 monitoring network to constrain the Indian land fluxes. *Atmospheric Environment* 218(1), 117003, https://doi.org/10.1016/j.atmosenv.2019.117003

Newman, S., Xu, X., Affek, H. P., Stolper, E., & Epstein, S. (2008). Changes in mixing ratio and isotopic composition of CO_2 in urban air from the Los Angeles basin, California, between 1972 and 2003. *Journal of Geophysical Research: Atmospheres*, 113(D23). https://doi.org/10.1029/2008JD009999

Pang, J., Wen, X., & Sun, X. (2016). Mixing ratio and carbon isotopic composition investigation of atmospheric CO_2 in Beijing, China. *Science of Total Environment* 539, 322-330, DOI: 10.1016/j.scitotenv.2015.08.130.

Pataki, D. E., Ehleringer, J. R., Flanagan, L. B., Yakir, D., Bowling, D. R., Still, C. J., ... & Berry, J. A. (2003). The application and interpretation of Keeling plots in terrestrial carbon cycle research. Global biogeochemical cycles, 17(1).

Pataki, D.E., Bowling, D.R., Ehleringer, J.R., & Zobitz, J.M. (2006). High resolution atmospheric monitoring of urban carbon dioxide sources. *Geophysical Research Letters* 33, 1–5, https://doi.org/10.1029/2005GL024822.

Sharma, N., Dadhwal, V. K., Kant, Y., Mahesh, P., Mallikarjun, K., Gadavi, H., Sharma, A., & Ali, M. M. (2014). Atmospheric CO_2 variations in two contrasting environmental sites over India. *Air soil and water Research*, 7, ASWR-S13987, https://doi.org/10.4137/ASWR.S13987.

763 Smith, H. J., Fischer, H., Wahlen, M., Mastroianni, D., & Deck, B. (1999). Dual modes of the
764 carbon cycle since the Last Glacial Maximum. *Nature*, 400 (6741), 248-250.
765
766 Sreenivas, G., Mahesh, P., Subin, J., Kanchana, A. L., Rao, P. V. N., & Dadhwal, V. K. (2016).
767 Influence of meteorology and interrelationship with greenhouse gases (CO_2 and CH_4) at a
768 suburban site of India. *Atmospheric Chemistry and Physics* 16, 3953-3967,
769 doi.org/10.5194/acp-16-3953-2016, 2016.
770
771 Sturm, P., Leuenberger, M., Valentino, F.L., Lehmann, B., & Ihly, B. (2006). Measurements of
772 CO_2, its stable isotopes, O_2/N_2, and Rn-222 at Bern, Switzerland. *Atmospheric Chemistry and*
773 *Physics*. 6, 1991-2004, https://doi.org/10.5194/acp-6-1991-2006, 2006.
774
775 Stull, R.B. (1988) An Introduction to Boundary Layer Meteorology. Kluwer Academic
776 Publishers, Dordrecht, Boston and London, 666 p. http://dx.doi.org/10.1007/978-94-009-3027-8.
777
778
779 Thoning, K. W., Tans, P. P., & Komhyr, W. D. (1989). Atmospheric carbon dioxide at Mauna
780 Loa Observatory: 2. Analysis of the NOAA GMCC data, 1974–1985. Journal of Geophysical
781 Research: Atmospheres, 94 (D6), 8549-8565.
782
783 Tiwari, Y. K., Vellore, R. K., Kumar, K. R., van der Schoot, M., & Cho, C. H. (2014). Influence
784 of monsoons on atmospheric CO_2 spatial variability and ground-based monitoring over India.
785 *Science of The Total Environment*, 490, 570-578, https://doi.org/10.1016/j.scitotenv.2014.05.045
786
787 Valsala, V., Tiwari, Y. K., Pillai, P., Roxy, M., Maksyutov, S., & Murtugudde, R. (2013).
788 Intraseasonal variability of terrestrial biospheric CO_2 fluxes over India during summer
789 monsoons. *Journal of Geophysical Research-Biogeosciences*, 118 (2), 752-769,
790 https://doi.org/10.1002/jgrg.20037.
791
792 Wada, R., Pearce, J.K., Nakayama, T., Matsumi, Y., Hiyama, T., Inoue, G., & Shibata, T.(2011).
793 Observation of carbon and oxygen isotopic compositions of CO_2 at an urban site in
794 Nagoya using mid-IR laser absorption spectroscopy. *Atmospheric Environment*, 45, 1168–1174,
795 https://doi.org/10.1016/j.atmosenv.2010.10.015.
796
797 Xu, W., Ruhl, M., Jenkyns, H.C., Hesselbo, S.P., Riding, J.B., et al. (2017). Carbon sequestration
798 in an expanded lake system during the Toarcian oceanic anoxic event. *Nature Geoscience*, 10,
799 129-134, doi: 10.1038/NGEO2871
800
801 Yakir, D. (2011). The paper trail of the ^{13}C of atmospheric CO_2 since the industrial revolution
802 period. *Environmental Research Letters* 6(3), 034007, http://dx.doi.org/10.1088/1748-
803 9326/6/3/034007.
804
805 Zhou, L., Conway, T. J., White, J. W., Mukai, H., Zhang, X., Wen, Y., Li, Jinlon., & MacClune,
806 K. (2005). Long-term record of atmospheric CO_2 and stable isotopic ratios at Waliguan
807 Observatory: Background features and possible drivers, 1991–2002. *Global Biogeochemical*
808 *Cycles*, 19(3), https://doi.org/10.1029/2004GB002430.

Zhou, L., J. W. C. White, T. J. Conway, H. Mukai, K. MacClune, X. Zhang, Y. Wen, and J. Li (2006), Long-term record of atmospheric CO_2 and stable isotopic ratios at Waliguan Observatory: Seasonally averaged 1991–2002 source/sink signals, and a comparison of 1998–2002 record to the 11 selected sites in the Northern Hemisphere, Global Biogeochem. Cycles, 20, GB2001,doi:10.1029/2004GB002431.

Zimnoch, M., Florkowski, T., Necki, J. M., & Neubert, R. E. (2004). Diurnal variability of $\delta^{13}C$ and $\delta^{18}O$ of atmospheric CO_2 in the urban atmosphere of Kraków, Poland. Isotopes in Environmental and Health Studies, 40, 129-143. https://doi.org/10.1080/10256010410001670989.